THE JOURNAL OF PHYSICAL CHEMISTRY C
A JOURNAL OF THE AMERICAN CHEMICAL SOCIETY

pubs.acs.org/JPCC

Article

# Effect of Excitonic Coupling and Disorder on Nonradiative Decay of Molecular Aggregates: A TD-DMRG Study

Zhao Zhang, Yijia Wang, Xiaoyan Zheng, Jiajun Ren,* Zhigang Shuai, and Weihai Fang

Cite This: *J. Phys. Chem. C* 2025, 129, 12520−12530

Read Online

ACCESS | Metrics & More | Article Recommendations | Supporting Information

**ABSTRACT:** Coherent exciton delocalization significantly impacts nonradiative decay processes in molecular aggregates, as evidenced by recent experimental and theoretical studies. Since delocalization is influenced by excitonic coupling strength, aggregate size, and both dynamic and static disorder, in this study, we employ the numerically exact time-dependent density matrix renormalization group algorithm combined with ab initio quantum chemistry calculations to investigate these effects on the nonradiative decay rate ($k_{nr}$) in J-aggregates of dihexylquaterrylene. Our findings reveal that $k_{nr}$ initially decreases and then increases with excitonic coupling strength, consistent with our previous study for a two-mode model. In the weak coupling regime, $k_{nr}$ decreases slightly with aggregate size, whereas in the strong coupling regime, it rises rapidly. Dynamic disorder generally enhances $k_{nr}$, except in the phonon-assisted regime, where it promotes exciton delocalization and reduces effective electron-vibration coupling. Static disorder consistently increases $k_{nr}$ by reducing the energy gap and localizing the exciton. These results provide valuable insights into optimizing excitonic coupling and minimizing disorder to enhance the photoluminescence quantum efficiency of molecular aggregates.

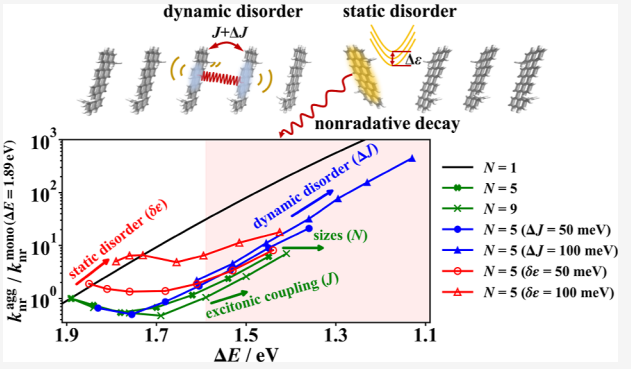




## INTRODUCTION

The study of aggregation effects on molecular photophysics has attracted significant research interest, as it is crucial not only for understanding fundamental physicochemical phenomena but also for industrial applications.[1,2] Key aggregation-induced effects, such as steric effects, polarization effects, excitonic coupling, and charge transfer states, play essential roles in different molecular aggregates.[3−10]

Recent experimental studies have shown that molecular aggregation can suppress the nonradiative decay rate $k_{nr}$, significantly enhancing near-infrared (NIR) photoluminescence quantum yield.[11−15] Notably, both the energy gap and $k_{nr}$ decrease from a single molecule to an aggregate.[12] This observation contradicts the well-established energy gap law, which predicts that $k_{nr}$ increases exponentially or even superexponentially as the energy gap decreases.[16,17] This novel finding is particularly exciting, as the development of efficient NIR luminescent molecules has long been hindered by fast nonradiative decay.[18]

To uncover the underlying mechanism, several theoretical studies have been conducted.[19,20] The steric effect, often invoked to explain aggregation-induced emission,[7,21] was ruled out, as the molecules studied are highly rigid.[11,12] Instead, excitonic coupling (EC, or exciton delocalization) has been proposed to reduce the effective electron-vibration coupling (EVC) strength, thereby lowering $k_{nr}$.[11,12,19,20] The role of EC in aggregate absorption and fluorescence spectra has been extensively studied, from Kasha's model[22] distinguishing J- and H-type aggregates to a series comprehensive works of Spano and co-workers.[23−26] A key effect of EC is the reduction in the 0-1 to 0-0 peak ratio in the emission spectrum of J-aggregates, reflecting a decrease in effective EVC strength.[23] However, the effect of EC on nonradiative processes did not gain much attention until recently.[19,20,27−31] Bonačić-Koutecký and coworkers proposed an analytical expression for $k_{nr}$ in molecular aggregates by incorporating EC into the energy gap law.[19,32] While this model successfully explains the decrease in $k_{nr}$ with increasing exciton delocalization in the weak EC regime, it assumed a purely excitonic model with harmonic potential energy surfaces and considers only the lowest electronic excited state. These assumptions are valid only in the strong EC regime, limiting the model's applicability across broader parameter spaces.

To address these limitations, our previous study employed the numerically exact time-dependent density matrix renormalization group (TD-DMRG) algorithm[33−36] to compute $k_{nr}$ in

Received: April 2, 2025
Revised: June 18, 2025
Accepted: June 20, 2025
Published: June 27, 2025

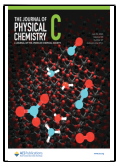




https://doi.org/10.1021/acs.jpcc.5c02232
J. Phys. Chem. C 2025, 129, 12520−12530

molecular aggregates using a microscopic electron-vibration coupled model.[20] The TD-DMRG algorithm has been successfully established as an accurate and efficient method for simulating chemical dynamics in electronic, vibrational, and vibronic systems.[37−45] We found that $k_{nr}$ exhibits a nonmonotonic dependence on EC strength: EC simultaneously reduces both the energy gap and the EVC strength, but these effects compete in determining the overall rate. The dominant factor determines whether $k_{nr}$ increases or decreases. Although this study provided a comprehensive physical picture, it was primarily based on a simplified two-mode model (one promoting mode plus one accepting mode). Additionally, real molecular aggregates, unlike covalently linked systems, are subject to structural fluctuations and imperfections due to weak noncovalent intermolecular interactions. Therefore, besides intramolecular vibrations, intermolecular vibrations (dynamic disorder) and local defects (static disorder) likely play critical roles in determining optoelectronic properties,[46−53] which were not fully explored in previous studies on nonradiative decay.

Therefore, in this study, we complement our previous study in three key aspects: (i) we constructed an electron-vibration coupled model for dihexylquaterrylene based on ab initio quantum chemistry calculations. This molecule (shown in Figure 1) has been experimentally observed to violate the energy gap law upon aggregation.[12] Using this more realistic model, we reassessed our prior findings. (ii) We investigated how intermolecular EVC influences $k_{nr}$. (iii) We examined the impact of static disorder on $k_{nr}$. Given the quantum many-body nature of electron-vibration coupled problems, we employed the TD-DMRG algorithm developed in our previous studies[35,39] to obtain nearly exact results. Our findings confirm that the previously observed nonmonotonic dependence of $k_{nr}$ on EC strength still holds, validating that the essential physics has already been captured by the two-mode model. We further found that the effect of intermolecular EVC on $k_{nr}$ depends on the coupling regime, it can either increase or decrease $k_{nr}$. In contrast, static disorder consistently increases $k_{nr}$. These insights deepen our understanding of how excitonic coupling, electron-vibration coupling, and disorder influence nonradiative decay processes in molecular aggregates.

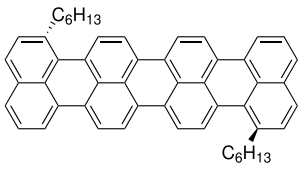


**Figure 1.** The Chemical formula of 1,1′-dihexylquaterrylene.

## METHODS

**Construction of Model Hamiltonian.** The Holstein−Peierls model is widely used to study excited-state dynamics, charge and exciton transport, and spectroscopy in molecular aggregates and molecular materials.[54−57] It consists of three components: the pure electronic Hamiltonian, intramolecular EVC, and intermolecular EVC.

$$\hat{H} = \hat{H}_e + \hat{H}_{intra} + \hat{H}_{inter} \quad (1)$$

**Holstein Hamiltonian.** The Holstein Hamiltonian, which includes only intramolecular EVC, is expressed as

$$\hat{H}_H = \hat{H}_e + \hat{H}_{intra} \quad (2)$$

$$\hat{H}_e = \sum_i \varepsilon_i |i\rangle\langle i| + \sum_{i\neq j} J_{ij} |i\rangle\langle j| \quad (3)$$

$$\hat{H}_{intra} = \sum_{in} \omega_{in} b_{in}^{\dagger} b_{in} + \sum_{in} g_{in}\omega_{in} |i\rangle\langle i|(b_{in}^{\dagger} + b_{in}) + \sum_{in} g_{in}^2 \omega_{in} |i\rangle\langle i| \quad (4)$$

where $|i\rangle$ represents the local excited state of the $i$th monomer with an adiabatic excitation energy $\varepsilon_i$. $J_{ij}$ denotes the excitonic coupling between monomers. $b_{in}^{\dagger}/b_{in}$ represents the bosonic creation/annihilation operator of the $n$th intramolecular mode of the $i$th molecule, with frequency $\omega_{in}$ and dimensionless EVC strength $g_{in}$.

The parameters $\varepsilon_i$, $g_{in}$, and $\omega_{in}$ were extracted from ab initio quantum chemistry calculations for a single dihexylquaterrylene molecule. The optimized geometries (Figure S1 in the Supporting Information) and electronic structures of the $S_0$ and $S_1$ states were computed using density functional theory (DFT) and time-dependent DFT (TD-DFT) by Gaussian 16.[58] The solvent environment was modeled via the integral equation formalism of the polarizable continuum model.[59] Vertical excitation energies were calculated using the corrected linear response approach,[60] employing three density functionals: B3LYP,[61] ωB97XD,[62] and optimally tuned[63] LC-PBE*[64] with $\omega$ = 0.1523, in conjunction with the 6-31G(d) basis set. The Molecular Material Property Prediction Package (MOMAP)[65,66] was used to compute intramolecular EVC strengths, absorption and fluorescence spectra, as well as radiative and nonradiative decay rates of monomer. By comparing with the experimental absorption and fluorescence spectra in dilute solutions,[12] we found that the optimally tuned LC-PBE* functional provided the best agreement (Figure S2). Therefore, its parameters were used to construct the aggregate model. The energy gap and reorganization energy of monomer is 1.89 eV and 141 meV, respectively.

Since dihexylquaterrylene is a rigid molecule, the Duschinsky rotation effect and vibrational frequency differences between the ground and excited states are small and thus neglected. The excited-state vibrational frequencies were used for all calculations. To further simplify the model, we retained only vibrational modes with significant contributions to nonradiative decay process, based on the criteria: (i) reorganization energy $\lambda_n > 20$ cm$^{-1}$, or (ii) nonadiabatic coupling $V_n = \langle S_1|\partial/\partial q_n|S_0\rangle$ among the largest $k$ terms, ensuring $\sum_n^k V_n^2\omega_n / \sum_n^{3N-6} V_n^2\omega_n > 0.9$. The reorganization energies of truncated modes were redistributed to the closest retained mode. This truncation reduced the number of vibrational modes from 192 to 46. The reorganization energy $\lambda_n$ of each mode with respect to $\omega_n$ is shown in Figure S3. Convergence tests for the time correlation function of nonradiative decay rates with respect to the number of retained modes are shown in Figure S4 of Supporting Information. The parameters $\omega_n$, $\lambda_n$, and $V_n$ are summarized in Table S1.

With regard to intermolecular excitonic coupling, the packing structure of dihexylquaterrylene aggregates in poor solvents remains unknown,[12] so we consider artificial one-dimensional aggregates with nearest-neighbor excitonic coupling. The coupling strength is estimated using a $\pi-\pi$ stacked


https://doi.org/10.1021/acs.jpcc.5c02232
J. Phys. Chem. C 2025, 129, 12520−12530

dimer model. The technical details are provided in Supporting Information Section S1. The optimized $\pi-\pi$ distance ($Z$-direction) is 3.6 Å, consistent with typical stacking distances of 3−4 Å. Since the transition dipole moment of monomer lies along the molecular long axis, the excitonic coupling switches from positive (H-type) to negative (J-type) when the displacement along the long axis exceeds 8 Å. As shown in Figure S5b, the maximum J-type coupling occurs at a displacement of ∼14 Å, with values of −69.5, −58.4, and −52.2 meV for $Z$ = 3.0, 3.6, and 4.0 Å, respectively. The top and side views of the dimer are presented in Figure S5c. To investigate the effect of excitonic coupling in a relatively large parameter space, we vary its strength from 0 to 300 meV.

**Peierls Terms.** Intermolecular vibrations introduce additional Hamiltonian terms, known as Peierls terms or dynamic disorder

$$\hat{H}_{\text{inter}} = \sum_i \omega_{i,\text{inter}} d_i^\dagger d_i + \sum_i g_{i,\text{inter}} \omega_{i,\text{inter}} (d_i^\dagger + d_i) (|i\rangle\langle i+1| + |i+1\rangle\langle i|) \tag{5}$$

where $d_i^\dagger$ and $d_i$ denote bosonic creation and annihilation operators for intermolecular vibrational modes between the $i$th and $(i+1)$th molecules. The mode frequency is set to 50 $\text{cm}^{-1}$, and the EVC strength is denoted as $g_{i,\text{inter}}$. Intermolecular EVC induces thermal fluctuations in the excitonic coupling strength, characterized by its standard deviation

$$\Delta J = g_{\text{inter}} \omega_{\text{inter}} \sqrt{\coth(\omega_{\text{inter}}/2k_B T)} \tag{6}$$

**Static Disorder.** Static disorder is modeled phenomenologically by assigning a Gaussian distribution to the local excitation energy $\varepsilon_0$

$$\varepsilon = \varepsilon_0 + \delta\varepsilon \tag{7}$$

$$p(\delta\varepsilon) = \frac{1}{\sqrt{2\pi}\sigma} \exp\left[-\frac{1}{2}\left(\frac{\delta\varepsilon}{\sigma}\right)^2\right] \tag{8}$$

The static disorder parameter $\delta\varepsilon$ is sampled according to this distribution, and ensemble-averaged observables are obtained using 50,000 realizations.

**Calculation of Nonradiative Decay Rate by TD-DMRG.** As a direct extension of single-molecule theory,[67,68] Fermi's golden rule is still adopted to calculate nonradiative decay rates and spectra in molecular aggregates.[9,20] It assumes that (i) the nonadiabatic coupling responsible for transitions between excited state and ground state is weak. (ii) Vibrational relaxation to the lowest vibronic state occurs faster than decay to the ground state, ensuring thermal equilibrium in the initial state. Under these assumptions, the nonradiative decay rate in the time domain is given by[9,20]

$$k_{\text{nr}}(\varepsilon_0) = \int_{-\infty}^{\infty} e^{i\varepsilon_0 t} C(t)\, dt \tag{9}$$

$$C(t) = \langle \hat{H}_1(t)\hat{H}_1\rangle_T = \text{Tr}\left(\frac{e^{-\beta\hat{H}_i}}{Z(\beta)} e^{i\hat{H}_i t}\hat{H}_1 e^{-i\hat{H}_i t}\hat{H}_1\right) \tag{10}$$

$$\hat{H}_i = \hat{H} - \varepsilon_0 \tag{11}$$

$$\hat{H}_f = \sum_{in} \omega_{in} b_{in}^\dagger b_{in} + \sum_i \omega_{i,\text{inter}} d_i^\dagger d_i = \hat{H}_v \tag{12}$$

where $Z(\beta) = \text{Tr}(e^{-\beta\hat{H}_i})$ is the partition function with inverse temperature $\beta = 1/k_B T$. The coupling operator $\hat{H}_1$ incorporates all nonadiabatic coupling operators across the molecular system

$$\hat{H}_1 = \sum_{in} - V_{in} |\text{GS}\rangle\langle i| \frac{\partial}{\partial q_{in}} + \text{h. c.} \tag{13}$$

where $|\text{GS}\rangle$ represents the electronic ground state.

To compute the time correlation function $C(t)$ in eq 10, we employ the numerically exact TD-DMRG algorithm. TD-DMRG approximates the exponentially large coefficient tensor as a low-rank matrix product state (MPS)[69,70]

$$|\Psi\rangle = \sum_{\{\sigma\}} C_{\sigma_1\sigma_2\cdots\sigma_N} |\sigma_1\sigma_2\cdots\sigma_N\rangle \tag{14}$$

$$\simeq \sum_{\{\sigma\},\{a\}} A[1]^{\sigma_1}_{a_1} A[2]^{\sigma_2}_{a_1 a_2} \cdots A[N]^{\sigma_N}_{a_{N-1}} |\sigma_1\sigma_2\cdots\sigma_N\rangle \tag{15}$$

where $|\sigma_i\rangle$ is the local basis function for the $i$th degree of freedom. The key advantage of TD-DMRG is its ability to handle hundreds or even thousands of vibrational modes with polynomial computational scaling. Meanwhile, the accuracy of TD-DMRG can be systematically improved by increasing the bond dimension $M$ (the size of $a_i$), to approach the exact limit. To obtain the initial thermal equilibrium state, we use the purification method.[39,71,72] This purification method introduces an auxiliary $Q$ space, identical to the physical $P$ space, to define a purified thermal wave function $|\Psi_\beta\rangle$ in the expanded Hilbert space $P \otimes Q$

$$|\Psi_\beta\rangle = \sum_{\{\sigma\},\sigma_i=\tilde{\sigma}_i} \frac{e^{-\beta\hat{H}/2}}{\sqrt{Z(\beta)}} |\sigma_1\cdots\sigma_N\rangle_P |\tilde{\sigma}_1\cdots\tilde{\sigma}_N\rangle_Q \tag{16}$$

$$\rho_\beta = \text{Tr}_Q |\Psi_\beta\rangle\langle\Psi_\beta| \tag{17}$$

where $|\tilde{\sigma}_i\rangle$ is the local basis function of the $i$th DoF in the auxiliary $Q$ space. $\rho_\beta$ is the thermal equilibrium density matrix. The purified wave function $|\Psi_\beta\rangle$ is obtained by evolving the imaginary-time Schrödinger equation from $t = 0$ ($|\Psi(0)\rangle = |\Psi_0\rangle$) to $t = -i\beta/2$ ($|\Psi(-i\beta/2)\rangle = |\Psi_\beta\rangle$). The initial state $|\Psi_0\rangle$ corresponds to a maximally mixed state at infinite high temperature ($\beta = 0$)

$$|\Psi_0\rangle = \prod_i \left(\sum_{\sigma_i,\sigma_i=\tilde{\sigma}_i} \frac{1}{\sqrt{d}} |\sigma_i\rangle|\tilde{\sigma}_i\rangle\right) \tag{18}$$

where $d$ is the size of the local basis functions. For simplicity, we assume each DoF has the same basis size, although in practice they can be different. It is straightforward to verify that $\text{Tr}_Q |\Psi_0\rangle\langle\Psi_0| = \hat{I}/d^N$, which corresponds to the correct density matrix at $\beta = 0$. The initial state $|\Psi_0\rangle$ can be represented as an MPS with bond dimension $M = d$. Once $|\Psi_\beta\rangle$ is obtained after imaginary-time evolution, real-time evolution is performed to compute $C(t)$. Both imaginary-time and real-time evolutions in TD-DMRG use the projector-splitting algorithm.[73] Further technical details can be found in our previous review[35] and other excellent refs 33, 34, and 36.

TD-DMRG calculations were performed using the open-source package Renormalizer,[74] developed in our group. The computational parameters were set as follows: the time step size is set to 0.5 fs, and the total evolution time to calculate $k_{\text{nr}}$


https://doi.org/10.1021/acs.jpcc.5c02232
J. Phys. Chem. C 2025, 129, 12520−12530

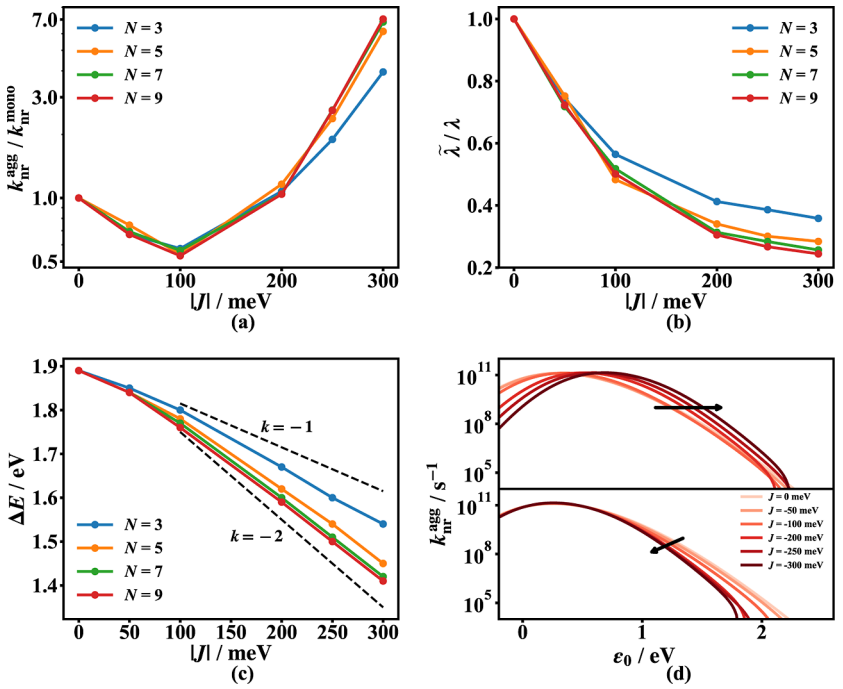


**Figure 2.** (a) The nonradiative decay rate of one-dimensional J-aggregates over that of monomer $k_{nr}^{agg}/k_{nr}^{mono}$ with different excitonic coupling strength $J$ simulated by the time-dependent density matrix renormalization group algorithm. (b) The effective reorganization energy $\tilde{\lambda}$ of aggregates with different $J$ obtained from vibrational distortion field. $\lambda$ is the monomer reorganization energy. (c) The energy gap $\Delta E$ of aggregates with different $J$. Different colors indicate different number of molecules. (d) The spectrum of nonradiative decay rate of aggregates $k_{nr}$ with respect to the local excitation energy $\varepsilon_0$. In the lower panel, the shift of energy gap is subtracted to show the width narrowing phenomena.

is 120 fs. The bond dimension $M$ is set to 32. The maximal local bosonic energy levels $d$ is truncated to 10 for intramolecular modes and to 30 for intermolecular modes. A phenomenological Gaussian broadening function $g(t) = \exp(-\eta^2 t^2/2)$ with $\eta$ = 0.2 eV is adopted to make $C(t)$ converge.

Finally, it should be mentioned that for the sake of simplicity, we adopted the site-based representation of the Holstein (or Holstein−Peierls) model throughout our calculations, as shown in eqs 3−5. In the weak coupling regime, this localized site-based representation is both natural and computationally efficient, typically allowing faster convergence with respect to the bond dimension. Conversely, in the strong excitonic coupling regime, a delocalized representation after Fourier transform (for both electronic states and vibrational modes) may be more advantageous due to the intrinsic delocalization of the vibronic wave function. To ensure the reliability of our results even under strong coupling conditions, we employed sufficiently large bond dimensions to guarantee convergence of the correlation functions.

**Features to Characterize Exciton in Molecular Aggregates.** The novel photophysical properties of molecular aggregates arise from the emergence of new excited states upon aggregation. The excited states can be coherently delocalized over multiple molecules, forming delocalized excitons. To characterize excitons in molecular aggregates, we consider key features including the energy gap, vibrational distortion field, and exciton delocalization length.

According to the energy gap law for single molecules,[16] $k_{nr}$ is primarily influenced by the energy gap and EVC strength (or reorganization energy). We expect these factors to remain critical in molecular aggregates. The energy gap of aggregates was obtained from the shift of the nonradiative spectrum.

The vibrational distortion field (VDF) describes how geometric structures distort around a local excitation.[25] Excitons coupled to such distortions are referred to as exciton polarons.[23] The VDF is defined as

$$\tilde{g}_n(r) = \frac{1}{2}\langle \sum_i |i\rangle\langle i|(b_{i+r,n}^{\dagger} + b_{i+r,n})\rangle_T \tag{19}$$

where $|i\rangle\langle i|$ denotes the local electronic excitation at the $i$th molecule, and $(b_{i+r,n}^{\dagger} + b_{i+r,n})$ represents the nuclear displacement of the $n$th mode at a distance $r$, with $\langle\rangle_T$ indicating thermal averaging. In the fully localized limit ($|\Psi\rangle = |i\rangle$), $\tilde{g}_n(r) = g_n\delta_{r0}$, meaning only the vibrational mode at the excited molecule is distorted, same as a single molecule. In the fully delocalized limit $\left(|\Psi\rangle = \frac{1}{\sqrt{N}}\sum_i |i\rangle\right)$, $\tilde{g}_n(r) = \frac{1}{\sqrt{N}}g_n$, indicating that distortions are evenly spread over all molecules with reduced displacement. Thus, VDF provides insight into exciton delocalization and can also be used to estimate the effective reorganization energy

$$\tilde{\lambda} = \sum_{r,n} \omega_n \tilde{g}_n(r)^2 \tag{20}$$

However, we found that for models with intermolecular vibrations, VDF alone is insufficient to characterize reorganization energy with intermolecular vibrations. Therefore, we proposed a new definition of effective reorganization energy, which is

$$\tilde{\lambda} = \mathrm{Tr}(\hat{H}_v\rho_v) - \mathrm{Tr}(\hat{H}_v\rho_v^{eq}) \tag{21}$$

$$\rho_v = \mathrm{Tr}_e(\rho_{ev}^{eq}) \tag{22}$$



https://doi.org/10.1021/acs.jpcc.5c02232
J. Phys. Chem. C 2025, 129, 12520−12530

The first term on the right-hand side represents the vibrational energy in equilibrium with the electronic excited state, while the second term corresponds to that in equilibrium with the electronic ground state. Their difference quantifies the vibrational reorganization to the electronic transition. For a fully localized exciton, the effective reorganization energy is $\tilde{\lambda} = \lambda$, while for a fully delocalized exciton, it scales as $\tilde{\lambda} = \lambda/N$, correctly recovering the limiting cases. We found that for intramolecular vibrations, both definitions in eqs 20 and 21 yield consistent results. However, for intermolecular vibrations, the second definition provides a more reasonable description (see Supporting Information Section S2).

The exciton delocalization length (EDL) quantifies how far an exciton spreads in real space. Besides VDF, other definitions based on the electronic reduced density matrix have been proposed.[75−77] We mainly use the one

$$L = \frac{(\sum_{ij}|\rho_{ij}|)^2}{N\sum_{ij}|\rho_{ij}|^2}, \qquad 1 \le L \le N \tag{23}$$

where $\rho_{ij}$ is the electronic reduced density matrix. In the fully localized limit, $\rho_{ij} = \frac{1}{N}\delta_{ij}$, yielding the minimum $L = 1$. In the fully delocalized limit, $\rho_{ij} = \frac{1}{N}$, yielding the maximum $L = N$. The numerical comparison of different definitions of EDL is shown in Supporting Information Section S3.

Together, energy gap $\Delta E$, effective reorganization energy $\tilde{\lambda}$, and exciton delocalization length $L$ provide a rather comprehensive picture of exciton behavior in molecular aggregates.

## RESULTS AND DISCUSSION

In this section, we show the effects of excitonic coupling, aggregate size, dynamic disorder, and static disorder on $k_{nr}$ in J-aggregates.

**Effect of Excitonic Coupling on $k_{nr}$.** Figure 2a shows the nonradiative decay rate of aggregates over that of monomer $k_{nr}^{agg}/k_{nr}^{mono}$ with different EC strengths. Initially, $k_{nr}^{agg}/k_{nr}^{mono}$ decreases and then increases, consistent with our previous findings for a two-mode model.[20] The turning point $J = 100$ meV is between $0.5\lambda$ and $\lambda$, approximately at $J \sim 0.7\lambda$. To understand this behavior, we calculated the effective reorganization energy $\tilde{\lambda}$ and energy gap $\Delta E$ shown in Figure 2b,c, both of which decrease monotonically with increasing EC. The decrease in $\tilde{\lambda}$ and $\Delta E$ are also reflected in the $k_{nr}$ spectrum as a function of the monomer's local excitation energy $\varepsilon_0$ (Figure 2d). Specifically: (i) the spectrum is blue-shifted, meaning $k_{nr}$ increases at the same $\varepsilon_0$, due to a red shift in the energy gap upon aggregation. (ii) After subtracting the energy gap reduction, the spectrum narrows, indicating a decrease in effective EVC with increasing EC. Since energy gap reduction tends to increase $k_{nr}$, while EVC reduction suppresses it, the overall trend of $k_{nr}$ depends on which effect dominates. As shown in Figure 2b,c, in the weak EC regime, $\tilde{\lambda}$ decreases rapidly, while $\Delta E$ reduction is modest, leading to a net decrease in $k_{nr}^{agg}/k_{nr}^{mono}$. Conversely, in the strong EC regime, $\tilde{\lambda}$ stabilizes at approximately $1/N$ of the monomer value $\lambda$, whereas $\Delta E$ decreases linearly with EC (with slopes of $-1$ for dimer and $-2$ for infinitely long chain). Thus, energy gap reduction dominates, causing $k_{nr}^{agg}/k_{nr}^{mono}$ to increase. Figure 3 shows the VDF of the mode with the strongest EVC ($\omega$ = 1640 cm$^{-1}$, $g = 0.47$) for aggregates with $N = 9$, spanning from weak to strong EC. The excitation is centered on the fifth molecule. As expected, at small $J$, the VDF, which characterizes the excitonic polaron profile, is highly localized and the effective EVC is close to that of monomer. As $J$ increases, it progressively delocalizes and the effective EVC decreases accordingly.

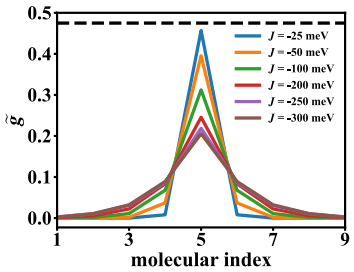


**Figure 3.** Vibrational distortion field profile of the mode with frequency $\omega$ = 1640 cm$^{-1}$ and electron-vibration coupling $g = 0.47$ for aggregates of $N = 9$, ranging from weak to strong excitonic coupling strength. The fifth molecule is excited. The dashed line represents the original $g$ of the monomer.

The physical picture in the strong EC regime ($J \gg \lambda$) is simple, illustrated in Figure 4 for a dimer (similar to Figure 11 in our recent review ref 9). The exciton is fully delocalized over two molecules, forming adiabatic electronic wave functions $|1\rangle \pm |2\rangle$, where $|1\rangle$ and $|2\rangle$ are diabatic localized states. This leads to two adiabatic potential energy surfaces (PESs) with normal modes $q^{\pm} = q_1 \pm q_2$ of the same frequency $\omega$. The energy separation between these PESs is $2J$, which, in the strong EC regime, is large enough to ignore the nonadiabatic coupling between them. Consequently, only the lower adiabatic state contributes, and its displacement relative to the ground state PES is reduced to $1/\sqrt{2}$ of the original $S_1$ PES. Since EVC is proportional to this displacement, it scales as $1/\sqrt{2}$. More generally, for an exciton delocalized over $N$ molecules, effective EVC scales as $1/\sqrt{N}$ of the monomer value, $g^{agg} = \frac{1}{\sqrt{N}}g^{mono}$. In this strong EC regime, since only the lowest excited-state PES is relevant and it is harmonic, the traditional energy gap law remains applicable but with a modified EVC as previously established in refs 11 and 19. Therefore, $k_{nr}$ follows the energy gap law in the strong EC regime, as shown in the right half of Figure 2a.

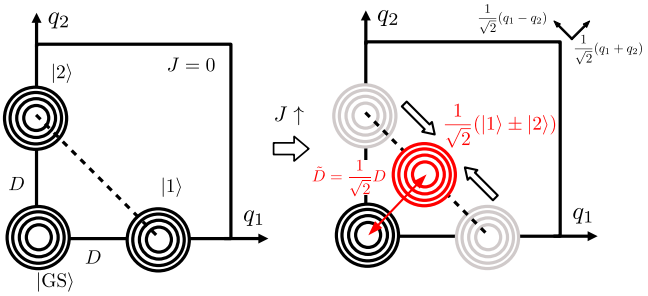


**Figure 4.** Schematic illustration of the evolution of potential energy contours of a dimer model as the excitonic coupling strength increases from $J = 0$ to the strong coupling limit. The displacement is reduced to $1/\sqrt{2}$ of its original value.

Furthermore, we show the impact of aggregate size on $k_{nr}$ in Figure 5a. When EC is weak, where the reduction in EVC dominates, $k_{nr}^{agg}/k_{nr}^{mono}$ decreases slightly with aggregate size $N$.



https://doi.org/10.1021/acs.jpcc.5c02232
J. Phys. Chem. C 2025, 129, 12520−12530

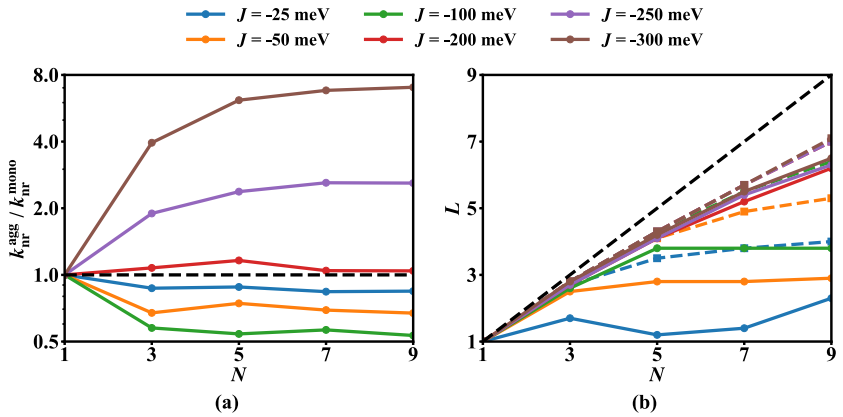


**Figure 5.** (a) Nonradiative decay rate $k_{nr}^{agg}/k_{nr}^{mono}$ and (b) exciton delocalization length $L$ of one-dimensional molecular aggregates as functions of aggregate size $N$. In (b), solid lines represent the results of vibronic model, while dashed lines represent the results of excitonic model. Different colors correspond to varying excitonic coupling strengths $J$.

Conversely, when EC is strong, where the reduction in energy gap dominates, $k_{nr}^{agg}/k_{nr}^{mono}$ increases significantly with $N$. In both cases, $k_{nr}^{agg}/k_{nr}^{mono}$ eventually converges to a plateau, indicating that the exciton delocalization length has reached its maximum due to either finite-size effects or EVC. Figure 5b presents the actual EDL as defined in eq 23. Compared to the purely electronic model $\hat{H}_e$, EDL is notably reduced when EVC is considered, particularly for small $J$. In addition to the definition of EDL in eq 23, two alternative definitions are compared in Figure S7, all of which show good consistency. Figure 5a is qualitatively consistent with Figure 2b in ref 19 by Bonačić-Koutecký and co-workers, confirming that their analytical equation based on a purely excitonic model correctly predicts the overall trend with respect to EDL. However, quantitatively, the results differ significantly. In our calculations for vibronic model, the maximum increase or decrease in $k_{nr}$ is within a few times, whereas the purely excitonic model exhibits a substantial overestimation, with variations spanning several orders of magnitude for similar EC strengths.[19]

**Effect of Intermolecular EVC on $k_{nr}$.** Intermolecular EVC introduces thermal fluctuations in excitonic coupling $\Delta J$, known as dynamic disorder or, more specifically, off-diagonal dynamic disorder. Previous studies have extensively explored its effects on charge and exciton transport,[47,50,56,78−80] identifying three regimes:[56] the phonon-assisted regime, the band regime, and the transient localization regime. Since exciton transport and nonradiative decay both depend on exciton delocalization, we examined how intermolecular EVC influences $k_{nr}$ within these regimes.

Figure 6 shows $k_{nr}$ for different EC strengths $J$ and intermolecular EVC strengths $\Delta J$: (i) in the phonon-assisted regime ($|J| < 50$ meV, $\Delta J < 25$ meV), $k_{nr}$ slightly decreases as $\Delta J$ increases. Here, the exciton is highly localized, and intermolecular vibrations instantaneously enhance EC strength, promoting exciton delocalization and reducing effective intramolecular EVC, thereby lowering $k_{nr}$. (ii) In the band regime ($|J| > 100$ meV, $\Delta J < 25$ meV), the exciton remains fully delocalized, and weak intermolecular EVC has little impact, leading to small changes in $k_{nr}$. (iii) In the transient localization regime ($\Delta J > 50$ meV), $k_{nr}$ increases sharply with $\Delta J$. Here, dynamic disorder disrupts exciton delocalization, increasing effective EVC and thus $k_{nr}$.

To further analyze these trends, we calculated $\tilde{\lambda}$ (eq 21) and $\Delta E$ as functions of $\Delta J$ (Figure 7). $\Delta E$ decreases monotonically

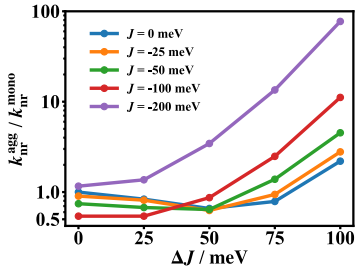


**Figure 6.** Nonradiative decay rate $k_{nr}^{agg}/k_{nr}^{mono}$ of a one-dimensional molecular chain with size $N = 5$ as a function of different intermolecular electron-vibration coupling strengths ($\Delta J$). Results for $N = 3$, 7, 9 are shown in Figure S8, which exhibit similar trends.

with $\Delta J$ (Figure 7a), an effect also observed in purely electronic models where the fluctuation of excitonic coupling follows a Gaussian distribution with standard deviation $\sigma = \Delta J$ (see Supporting Information Section S5, Figure S9). This energy gap reduction enhances $k_{nr}$. Meanwhile, $\tilde{\lambda}_{tot}$ generally increases with $\Delta J$ (Figure 7b), except in the phonon-assisted regime, aligning with trends in Figure 6. Decomposing $\tilde{\lambda}$ into intramolecular and intermolecular contributions (Figure 7c,d), we found that $\tilde{\lambda}_{intra}$ decreases with $\Delta J$, particularly when $J$ is small. In contrast, intermolecular $\tilde{\lambda}_{inter}$ increases rapidly, indicating that as intermolecular EVC strengthens, more electronic energy dissipates into intermolecular vibrations during vibrational relaxation.

**Effect of Static Disorder on $k_{nr}$.** In addition to intramolecular and intermolecular EVC, static disorder plays a crucial role in realistic molecular aggregates. A well-known effect is Anderson localization,[81] where low-energy states in a disordered system become spatially localized. We investigated the impact of static disorder on $k_{nr}$, finding that $k_{nr}^{agg}/k_{nr}^{mono}$ increases monotonically with disorder strength (Figure 8a). This trend arises from two key factors. First, as static disorder increases, excitons become more localized (Figure 8b), particularly when $|J| < \delta\varepsilon$, in line with Anderson localization. This localization increases EVC to values closer to that of a monomer (Figure 8c). Second, static disorder reduces the energy gap (Figure 8d), an effect also observed in purely electronic models (see Supporting Information Section S5, Figure S10). Both factors contribute to the observed increase in $k_{nr}$ with static disorder.



https://doi.org/10.1021/acs.jpcc.5c02232
J. Phys. Chem. C 2025, 129, 12520−12530

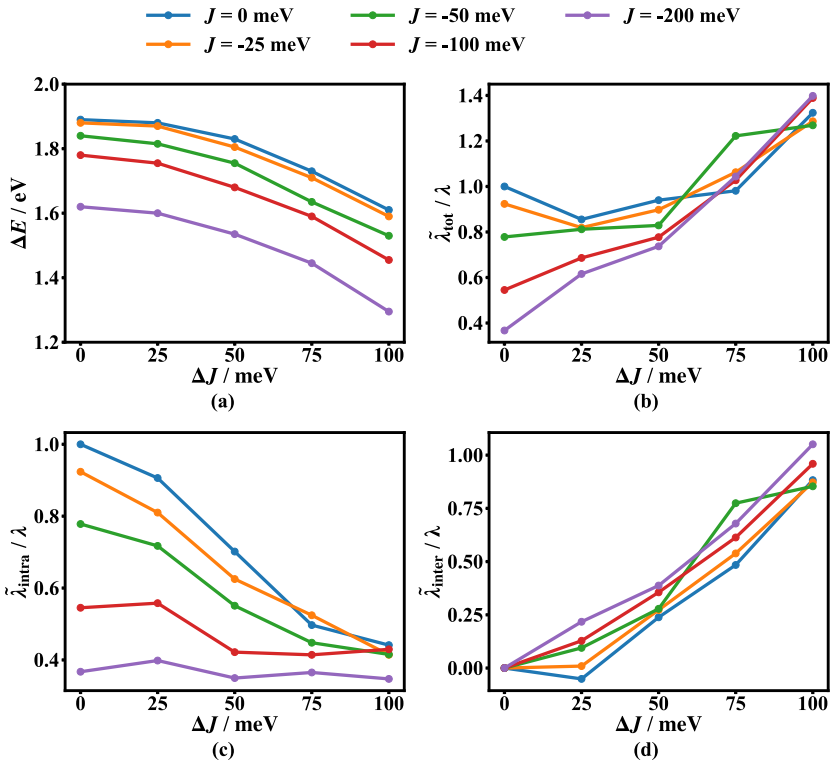


**Figure 7.** Energy gap $\Delta E$ and effective reorganization energy $\tilde{\lambda}$ of a one-dimensional molecular chain with size $N = 5$ as a function of different intermolecular electron-vibration coupling strengths $\Delta J$. (a) Energy gap (b) total reorganization energy (c) intramolecular reorganization energy (d) intermolecular reorganization energy.

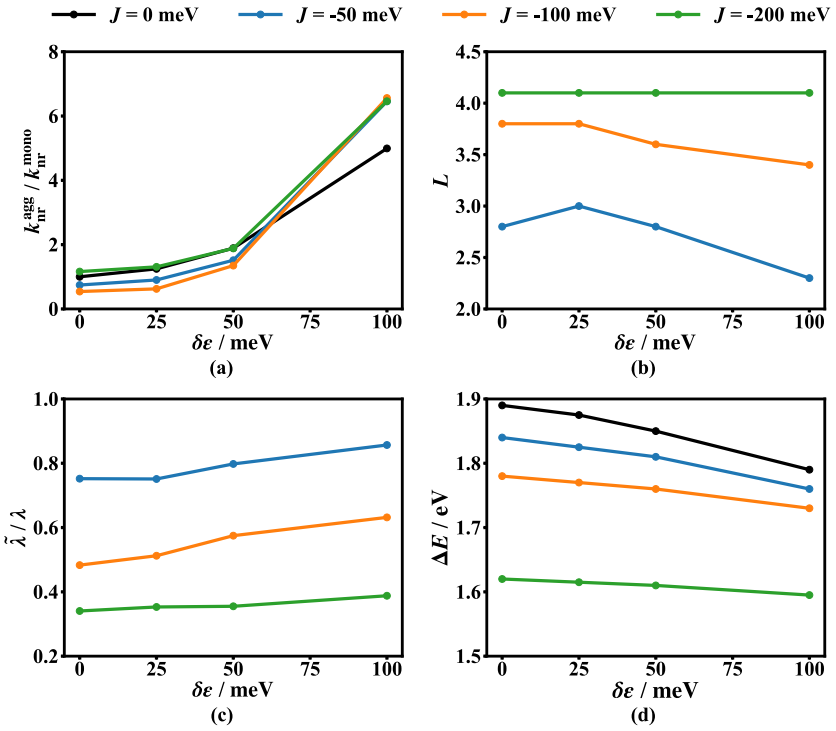


**Figure 8.** Effect of static disorder on nonradiative decay rate and excitonic structure of one-dimensional molecular aggregates with $N = 5$. (a) Nonradiative decay rate $k_{nr}^{agg}/k_{nr}^{mono}$. (b) Exciton delocalization length $L$. Different colors denote different excitonic coupling strength $J$. (c) Effective reorganization energy $\tilde{\lambda}$. (d) Energy gap $\Delta E$.

We gathered all $k_{nr}$ data under the influence of excitonic coupling, dynamic disorder, and static disorder and plotted them against the energy gap $\Delta E$ in Figure 9. The black line represents the monomer case, where $k_{nr}$ exhibits an exponential increase as $\Delta E$ decreases. With excitonic coupling, $k_{nr}$ is significantly reduced by nearly an order of magnitude for the



https://doi.org/10.1021/acs.jpcc.5c02232
J. Phys. Chem. C 2025, 129, 12520−12530

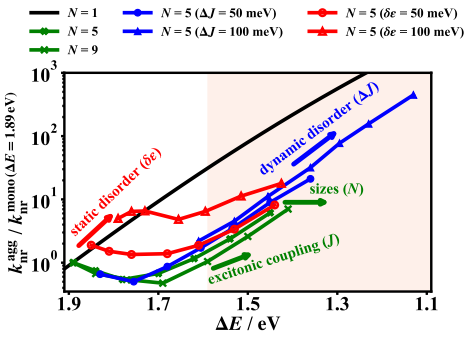


**Figure 9.** Nonradiative decay rate $k_{nr}$ as a function of the energy gap, considering the effects of excitonic coupling, aggregate size, dynamic disorder, and static disorder. The nonradiative decay rate of monomer at the energy gap $\Delta E$ = 1.89 eV is set as the unit. Along each line, the excitonic coupling strength gradually increases ($J$ = 0, −50, −100, −150, −200, −250, −300 meV). Green lines indicate the influence of excitonic coupling for different system sizes. Red lines indicate the influence of static disorder. Blue lines indicate the influence of dynamic disorder. The black line shows the monomer case. The shaded red region marks the near-infrared regime (>780 nm).

same $\Delta E$ (green curves). However, at large $J$, the slope of the curve eventually returns to that of monomer. As aggregate size increases, the EC effect is further enhanced due to the increased EDL. Static disorder shifts the entire curve upward (red curves), detrimental to luminescent properties. Dynamic disorder induces a substantial redshift in the luminescence wavelength but also increases $k_{nr}$ at the same $\Delta E$, causing the curve to enter the rising regime more rapidly (blue curves). Therefore, from the perspective of reducing $k_{nr}$, dynamic disorder is also detrimental.

Finally, we briefly discuss how our findings relate to experimental observations.[12] The apparent excitonic coupling deduced from experimental spectral shifts is approximately −200 meV, under the assumption of a one-dimensional packing structure.[12] First, according to our results (Figure 2), although −200 meV exceeds the optimal coupling (around −100 meV) that minimizes the nonradiative decay rate, the rate remains comparable to that of the monomer, even as the energy gap decreases from 1.89 to 1.59 eV ($N$ = 9). Experimentally, aggregation reduces the gap from 1.85 to 1.48 eV, with the nonradiative decay rate decreasing to 60% of the monomer. Compared to the experiments, our calculation results show a similar qualitative trend despite quantitative differences. Second, our ab initio calculations estimate the maximum excitonic coupling for a slip-stacked dimer to be between −70 and −50 meV, much smaller than the apparent value inferred from spectra. This discrepancy suggests that the observed large red shift in spectra is not solely due to excitonic coupling in one-dimension but may also involve other factors, such as two- or three-dimensional packing or polarization effects within the aggregate. These factors deserve further investigation.

## CONCLUSIONS

In this work, we constructed an electron-vibration coupled model for dihexylquaterrylene using ab initio quantum chemistry calculations and employed the highly accurate TD-DMRG algorithm to study the nonradiative decay rate of J-aggregates across a broad parameter space. By analyzing the energy gap, effective reorganization energy, and exciton delocalization length, we systematically explored the effects of excitonic coupling, aggregate size, dynamic disorder, and static disorder on the nonradiative decay rate.

Our results reveal that the nonradiative decay rate initially decreases and then increases with excitonic coupling strength, consistent with our previous study for a two-mode model. In the weak excitonic coupling regime, the decay rate decreases slightly with aggregate size, whereas in the strong coupling regime, it increases rapidly. Intermolecular EVC generally enhances the decay rate, except in the phonon-assisted regime, where it promotes exciton delocalization and reduces the effective EVC. Static disorder consistently increases the decay rate by simultaneously reducing the energy gap and increasing the reorganization energy. The detailed investigation of dynamic and static disorder, which was lacking in previous studies, is the main contribution of this work. These insights offer guidance for optimizing exciton delocalization to enhance the photoluminescence quantum efficiency of fluorescent molecular systems. Excitonic coupling should be carefully tuned: it must be strong enough to induce exciton delocalization but not so strong that the energy gap reduction dominates. The optimal coupling strength is approximately 0.5−1 of the monomer's reorganization energy. Additionally, disorder, whether dynamic or static, is detrimental as it generally increases nonradiative decay, highlighting the importance of a more ordered stacking arrangement.

A limitation of this study is the lack of detailed structural information on aggregates in poor solvents, requiring assumptions about parameters related to intermolecular packing, such as intermolecular coupling strength. This makes direct comparison with experiments difficult. Therefore, instead of focusing solely on dihexylquaterrylene aggregates, this work aims to provide a general understanding of nonradiative decay in molecular aggregates using a more realistic multimode electron-vibration coupling model. Future studies incorporating molecular dynamics simulations to determine the self-assembled structure would provide a further understanding of the structure−property relationship from first principles.

## ASSOCIATED CONTENT

### Supporting Information

The Supporting Information is available free of charge at https://pubs.acs.org/doi/10.1021/acs.jpcc.5c02232.

Quantum chemistry calculations and spectra of monomer; numerical comparison of different definitions of effective reorganization energy; numerical comparison of different definitions of exciton delocalization length; nonradiative decay rate with intermolecular electron-vibration coupling for different aggregate sizes; disorder-induced energy gap reduction in the excitonic model (PDF)

## AUTHOR INFORMATION

### Corresponding Author

**Jiajun Ren** − *Key Laboratory of Theoretical and Computational Photochemistry, Ministry of Education, College of Chemistry, Beijing Normal University, Beijing 100875, People's Republic of China;* orcid.org/0000-0002-1508-4943; Email: jjren@bnu.edu.cn

## Authors

**Zhao Zhang** − *Key Laboratory of Theoretical and Computational Photochemistry, Ministry of Education, College of Chemistry, Beijing Normal University, Beijing 100875, People's Republic of China*

**Yijia Wang** − *Key Laboratory of Cluster Science of Ministry of Education, Key Laboratory of Medicinal Molecule Science and Pharmaceutics Engineering of Ministry of Industry and Information Technology, Beijing Key Laboratory of Photoelectronic/Electro-Photonic Conversion Materials, School of Chemistry and Chemical Engineering, Beijing Institute of Technology, Beijing 100081, China*

**Xiaoyan Zheng** − *Key Laboratory of Cluster Science of Ministry of Education, Key Laboratory of Medicinal Molecule Science and Pharmaceutics Engineering of Ministry of Industry and Information Technology, Beijing Key Laboratory of Photoelectronic/Electro-Photonic Conversion Materials, School of Chemistry and Chemical Engineering, Beijing Institute of Technology, Beijing 100081, China;* orcid.org/0000-0002-6584-9596

**Zhigang Shuai** − *School of Science and Engineering, The Chinese University of Hong Kong, Shenzhen 518172, P. R. China*

**Weihai Fang** − *Key Laboratory of Theoretical and Computational Photochemistry, Ministry of Education, College of Chemistry, Beijing Normal University, Beijing 100875, People's Republic of China;* orcid.org/0000-0002-1668-465X

Complete contact information is available at: https://pubs.acs.org/10.1021/acs.jpcc.5c02232


## Notes

The authors declare no competing financial interest.

## ■ ACKNOWLEDGMENTS

This work is supported by the National Natural Science Foundation of China (Grant No. 22273005 and No. 22422301), the Innovation Program for Quantum Science and Technology (Grant No. 2023ZD0300200), NSAF (Grant No. U2330201), and the Fundamental Research Funds for the Central Universities.

## ■ REFERENCES


(1) Zhang, H.; Zhao, Z.; Turley, A. T.; Wang, L.; McGonigal, P. R.; Tu, Y.; Li, Y.; Wang, Z.; Kwok, R. T.; Lam, J. W.; et al. Aggregate science: from structures to properties. *Adv. Mater.* **2020**, *32*, 2001457.

(2) Bialas, D.; Kirchner, E.; Röhr, M. I.; Würthner, F. Perspectives in dye chemistry: a rational approach toward functional materials by understanding the aggregate state. *J. Am. Chem. Soc.* **2021**, *143*, 4500−4518.

(3) Popp, W.; Brey, D.; Binder, R.; Burghardt, I. Quantum dynamics of exciton transport and dissociation in multichromophoric systems. *Annu. Rev. Phys. Chem.* **2021**, *72*, 591−616.

(4) Dimitriev, O. P. Dynamics of excitons in conjugated molecules and organic semiconductor systems. *Chem. Rev.* **2022**, *122*, 8487−8593.

(5) Han, G.; Yi, Y. Molecular insight into efficient charge generation in low-driving-force nonfullerene organic solar cells. *Acc. Chem. Res.* **2022**, *55*, 869−877.

(6) Hernández, F. J.; Crespo-Otero, R. Modeling excited states of molecular organic aggregates for optoelectronics. *Annu. Rev. Phys. Chem.* **2023**, *74*, 547−571.

(7) Peng, Q.; Shuai, Z. Molecular mechanism of aggregation-induced emission. *Aggregate* **2021**, *2*, No. e91.

(8) Liang, W.; Wang, Y.-C.; Feng, S.; Zhao, Y. Chapter 15-Modeling the Photophysical Processes of Organic Molecular Aggregates with Inclusion of Intermolecular Interactions and Vibronic Couplings. In *Exploring Chemical Concepts Through Theory and Computation*; John Wiley & Sons, Ltd, 2024; pp 379−406.

(9) Shuai, Z.; Sun, Q.; Ren, J.; Jiang, T.; Li, W. Excited state structure and decay rates for aggregates. *Aggregate* **2025**, *6*, No. e70013.

(10) Wang, Z.; Xie, X.; Ma, H. Theoretical Investigation of Singlet Fission Processes in Organic Photovoltaics. *Wiley Interdiscip. Rev. Comput. Mol. Sci.* **2025**, *15*, No. e70002.

(11) Wei, Y.-C.; Wang, S. F.; Hu, Y.; Liao, L.-S.; Chen, D.-G.; Chang, K.-H.; Wang, C.-W.; Liu, S.-H.; Chan, W.-H.; Liao, J.-L.; et al. Overcoming the energy gap law in near-infrared OLEDs by exciton−vibration decoupling. *Nat. Photonics* **2020**, *14*, 570−577.

(12) Cravcenco, A.; Yu, Y.; Edhborg, F.; Goebel, J. F.; Takacs, Z.; Yang, Y.; Albinsson, B.; Borjesson, K. Exciton delocalization counteracts the energy gap: a new pathway toward NIR-emissive dyes. *J. Am. Chem. Soc.* **2021**, *143*, 19232−19239.

(13) Wei, Y.-C.; Kuo, K.-H.; Chi, Y.; Chou, P.-T. Efficient near-infrared luminescence of self-assembled platinum (II) complexes: from fundamentals to applications. *Acc. Chem. Res.* **2023**, *56*, 689−699.

(14) Zhao, J.; Gao, Y.; Huang, R.; Chi, C.; Sun, Y.; Xu, G.; Xia, X.-H.; Gou, S. Design of near-infrared-triggered metallo-photosensitizers via a self-assembly-induced vibronic decoupling strategy. *J. Am. Chem. Soc.* **2023**, *145*, 11633−11642.

(15) Fang, L.; Huang, R.; Gong, W.; Ji, Y.; Sun, Y.; Gou, S.; Zhao, J. A Self-Assembly-Induced Exciton Delocalization Strategy for Converting a Perylene Diimide Derivative from a Type-II to Type-I Photosensitizer. *Small* **2024**, *20*, 2307414.

(16) Englman, R.; Jortner, J. The energy gap law for radiationless transitions in large molecules. *Mol. Phys.* **1970**, *18*, 145−164.

(17) Nitzan, A. *Chemical Dynamics in Condensed Phases: Relaxation, Transfer, and Reactions in Condensed Molecular Systems*; Oxford University Press, 2024.

(18) Zampetti, A.; Minotto, A.; Cacialli, F. Near-infrared (NIR) organic light-emitting diodes (OLEDs): challenges and opportunities. *Adv. Funct. Mater.* **2019**, *29*, 1807623.

(19) Humeniuk, A.; Mitric, R.; Bonačić-Koutecký, V. Size dependence of non-radiative decay rates in J-aggregates. *J. Phys. Chem. A* **2020**, *124*, 10143−10151.

(20) Wang, Y.; Ren, J.; Shuai, Z. Minimizing non-radiative decay in molecular aggregates through control of excitonic coupling. *Nat. Commun.* **2023**, *14*, 5056.

(21) Mei, J.; Leung, N. L.; Kwok, R. T.; Lam, J. W.; Tang, B. Z. Aggregation-induced emission: together we shine, united we soar. *Chem. Rev.* **2015**, *115*, 11718−11940.

(22) Kasha, M. Energy transfer mechanisms and the molecular exciton model for molecular aggregates. *Radiat. Res.* **1963**, *20*, 55−70.

(23) Spano, F. C. The spectral signatures of Frenkel polarons in H- and J-aggregates. *Acc. Chem. Res.* **2010**, *43*, 429−439.

(24) Hestand, N. J.; Spano, F. C. Molecular aggregate photophysics beyond the Kasha model: novel design principles for organic materials. *Acc. Chem. Res.* **2017**, *50*, 341−350.

(25) Hestand, N. J.; Spano, F. C. Expanded theory of H-and J-molecular aggregates: the effects of vibronic coupling and intermolecular charge transfer. *Chem. Rev.* **2018**, *118*, 7069−7163.

(26) Ghosh, R.; Spano, F. C. Excitons and polarons in organic materials. *Acc. Chem. Res.* **2020**, *53*, 2201−2211.

(27) Scharf, B.; Dinur, U. Striking dependence of the rate of electronic radiationless transitions on the size of the molecular system. *Chem. Phys. Lett.* **1984**, *105*, 78−82.

(28) Celestino, A.; Eisfeld, A. Tuning nonradiative lifetimes via molecular aggregation. *J. Phys. Chem. A* **2017**, *121*, 5948−5953.

(29) Li, W.; Zhu, L.; Shi, Q.; Ren, J.; Peng, Q.; Shuai, Z. Excitonic coupling effect on the nonradiative decay rate in molecular aggregates: Formalism and application. *Chem. Phys. Lett.* **2017**, *683*, 507−514.

(30) Chen, X.-K.; Qian, D.; Wang, Y.; Kirchartz, T.; Tress, W.; Yao, H.; Yuan, J.; Hülsbeck, M.; Zhang, M.; Zou, Y.; et al. A unified description of non-radiative voltage losses in organic solar cells. *Nat. Energy* **2021**, *6*, 799−806.
(31) Kong, Y.; Wang, Y.-C.; Huang, X.; Liang, W.; Zhao, Y. Switching on/off phosphorescent or non-radiative channels by aggregation-induced quantum interference. *Aggregate* **2024**, *5*, No. e395.
(32) Bužančić Milosavljević, M.; Bonačić-Koutecký, V. Design of J-aggregates-like oligomers built from squaraine dyes exhibiting transparency in the visible regime and high fluorescence quantum yield in the NIR region. *Phys. Chem. Chem. Phys.* **2024**, *26*, 1314−1321.
(33) Ma, H.; Luo, Z.; Yao, Y. The time-dependent density matrix renormalisation group method. *Mol. Phys.* **2018**, *116*, 854−868.
(34) Borrelli, R.; Gelin, M. F. Finite temperature quantum dynamics of complex systems: Integrating thermo-field theories and tensor-train methods. *Wiley Interdiscip. Rev. Comput. Mol. Sci.* **2021**, *11*, No. e1539.
(35) Ren, J.; Li, W.; Jiang, T.; Wang, Y.; Shuai, Z. Time-dependent density matrix renormalization group method for quantum dynamics in complex systems. *Wiley Interdiscip. Rev. Comput. Mol. Sci.* **2022**, *12*, No. e1614.
(36) Ma, H.; Schollwöck, U.; Shuai, Z. *Density Matrix Renormalization Group (DMRG)-Based Approaches in Computational Chemistry*; Elsevier, 2022.
(37) Ronca, E.; Li, Z.; Jimenez-Hoyos, C. A.; Chan, G. K.-L. Time-step targeting time-dependent and dynamical density matrix renormalization group algorithms with ab initio Hamiltonians. *J. Chem. Theory Comput.* **2017**, *13*, 5560−5571.
(38) Greene, S. M.; Batista, V. S. Tensor-train split-operator Fourier transform (TT-SOFT) method: Multidimensional nonadiabatic quantum dynamics. *J. Chem. Theory Comput.* **2017**, *13*, 4034−4042.
(39) Ren, J.; Shuai, Z.; Kin-Lic Chan, G. Time-dependent density matrix renormalization group algorithms for nearly exact absorption and fluorescence spectra of molecular aggregates at both zero and finite temperature. *J. Chem. Theory Comput.* **2018**, *14*, 5027−5039.
(40) Yao, Y.; Sun, K.-W.; Luo, Z.; Ma, H. Full quantum dynamics simulation of a realistic molecular system using the adaptive time-dependent density matrix renormalization group method. *J. Phys. Chem. Lett.* **2018**, *9*, 413−419.
(41) Baiardi, A.; Reiher, M. Large-scale quantum dynamics with matrix product states. *J. Chem. Theory Comput.* **2019**, *15*, 3481−3498.
(42) Wang, K.; Xu, Y.; Xie, X.; Ma, H. Theoretical investigation of distal charge separation in a perylenediimide trimer. *J. Chem. Phys.* **2024**, *160*, 164303.
(43) Liu, S.; Peng, J.; Bao, P.; Shi, Q.; Lan, Z. Ultrafast excited-state energy transfer in phenylene ethynylene dendrimer: Quantum dynamics with the tensor network method. *J. Phys. Chem. A* **2024**, *128*, 6337−6350.
(44) Hino, K.; Kurashige, Y. Encoding a Many-body Potential Energy Surface into a Grid-Based Matrix Product Operator. *J. Chem. Theory Comput.* **2024**, *20*, 3839−3849.
(45) Wang, Y.; Benny, A.; Le Dé, B.; Chin, A. W.; Scholes, G. D. A numerically exact description of ultrafast vibrational decoherence in vibration-coupled electron transfer. *Proc. Natl. Acad. Sci. U.S.A.* **2025**, *122*, No. e2416542122.
(46) Troisi, A. Charge transport in high mobility molecular semiconductors: classical models and new theories. *Chem. Soc. Rev.* **2011**, *40*, 2347−2358.
(47) Ciuchi, S.; Fratini, S.; Mayou, D. Transient localization in crystalline organic semiconductors. *Phys. Rev. B: Condens. Matter Mater. Phys.* **2011**, *83*, 081202.
(48) Lee, C. K.; Moix, J.; Cao, J. Coherent quantum transport in disordered systems: A unified polaron treatment of hopping and band-like transport. *J. Chem. Phys.* **2015**, *142*, 164103.
(49) Aragó, J.; Troisi, A. Dynamics of the excitonic coupling in organic crystals. *Phys. Rev. Lett.* **2015**, *114*, 026402.
(50) Fratini, S.; Mayou, D.; Ciuchi, S. The transient localization scenario for charge transport in crystalline organic materials. *Adv. Funct. Mater.* **2016**, *26*, 2292−2315.
(51) Engelhardt, G.; Cao, J. Unusual dynamical properties of disordered polaritons in microcavities. *Phys. Rev. B* **2022**, *105*, 064205.
(52) Balzer, D.; Kassal, I. Mechanism of delocalization-enhanced exciton transport in disordered organic semiconductors. *J. Phys. Chem. Lett.* **2023**, *14*, 2155−2162.
(53) Brey, D.; Burghardt, I. Coherent Transient Localization Mechanism of Interchain Exciton Transport in Regioregular P3HT: A Quantum-Dynamical Study. *J. Phys. Chem. Lett.* **2024**, *15*, 1836−1845.
(54) Wang, Y.-C.; Zhao, Y. Effect of an underdamped vibration with both diagonal and off-diagonal exciton−phonon interactions on excitation energy transfer. *J. Comput. Chem.* **2019**, *40*, 1097−1104.
(55) Fetherolf, J. H.; Golež, D.; Berkelbach, T. C. A unification of the Holstein polaron and dynamic disorder pictures of charge transport in organic crystals. *Phys. Rev. X* **2020**, *10*, 021062.
(56) Li, W.; Ren, J.; Shuai, Z. A general charge transport picture for organic semiconductors with nonlocal electron-phonon couplings. *Nat. Commun.* **2021**, *12*, 4260.
(57) Bialas, A. L.; Spano, F. C. A Holstein−Peierls approach to excimer spectra: The evolution from vibronically structured to unstructured emission. *J. Phys. Chem. C* **2022**, *126*, 4067−4081.
(58) Frisch, M. J.; Trucks, G. W.; Schlegel, H. B.; Scuseria, G. E.; Robb, M. A.; Cheeseman, J. R.; Scalmani, G.; Barone, V.; Petersson, G. A.; Nakatsuji, H.; et al. *Gaussian 16*; Gaussian, Inc., 2019.
(59) Tomasi, J.; Mennucci, B.; Cammi, R. Quantum mechanical continuum solvation models. *Chem. Rev.* **2005**, *105*, 2999−3094.
(60) Caricato, M.; Mennucci, B.; Tomasi, J.; Ingrosso, F.; Cammi, R.; Corni, S.; Scalmani, G. Formation and relaxation of excited states in solution: A new time dependent polarizable continuum model based on time dependent density functional theory. *J. Chem. Phys.* **2006**, *124*, 124520.
(61) Lee, C.; Yang, W.; Parr, R. G. Development of the Colle-Salvetti correlation-energy formula into a functional of the electron density. *Phys. Rev. B: Condens. Matter Mater. Phys.* **1988**, *37*, 785.
(62) Chai, J.-D.; Head-Gordon, M. Long-range corrected hybrid density functionals with damped atom−atom dispersion corrections. *Phys. Chem. Chem. Phys.* **2008**, *10*, 6615−6620.
(63) Kronik, L.; Stein, T.; Refaely-Abramson, S.; Baer, R. Excitation gaps of finite-sized systems from optimally tuned range-separated hybrid functionals. *J. Chem. Theory Comput.* **2012**, *8*, 1515−1531.
(64) Jacquemin, D.; Moore, B.; Planchat, A.; Adamo, C.; Autschbach, J. Performance of an optimally tuned range-separated hybrid functional for 0−0 electronic excitation energies. *J. Chem. Theory Comput.* **2014**, *10*, 1677−1685.
(65) Niu, Y.; Li, W.; Peng, Q.; Geng, H.; Yi, Y.; Wang, L.; Nan, G.; Wang, D.; Shuai, Z. MOlecular MAterials Property Prediction Package (MOMAP) 1.0: a software package for predicting the luminescent properties and mobility of organic functional materials. *Mol. Phys.* **2018**, *116*, 1078−1090.
(66) Shuai, Z. Thermal vibration correlation function formalism for molecular excited state decay rates. *Chin. J. Chem.* **2020**, *38*, 1223−1232.
(67) Niu, Y.; Peng, Q.; Shuai, Z. Promoting-mode free formalism for excited state radiationless decay process with Duschinsky rotation effect. *Sci. China, Ser. B: Chem.* **2008**, *51*, 1153−1158.
(68) Niu, Y.; Peng, Q.; Deng, C.; Gao, X.; Shuai, Z. Theory of excited state decays and optical spectra: application to polyatomic molecules. *J. Phys. Chem. A* **2010**, *114*, 7817−7831.
(69) White, S. R. Density matrix formulation for quantum renormalization groups. *Phys. Rev. Lett.* **1992**, *69*, 2863.
(70) Schollwöck, U. The density-matrix renormalization group in the age of matrix product states. *Ann. Phys.* **2011**, *326*, 96−192.
(71) Verstraete, F.; Garcia-Ripoll, J. J.; Cirac, J. I. Matrix product density operators: Simulation of finite-temperature and dissipative systems. *Phys. Rev. Lett.* **2004**, *93*, 207204.


https://doi.org/10.1021/acs.jpcc.5c02232
J. Phys. Chem. C 2025, 129, 12520−12530

(72) Feiguin, A. E.; White, S. R. Finite-temperature density matrix renormalization using an enlarged Hilbert space. *Phys. Rev. B: Condens. Matter Mater. Phys.* **2005**, *72*, 220401.
(73) Haegeman, J.; Lubich, C.; Oseledets, I.; Vandereycken, B.; Verstraete, F. Unifying time evolution and optimization with matrix product states. *Phys. Rev. B* **2016**, *94*, 165116.
(74) Renormalizer. 2025, https://github.com/shuaigroup/Renormalizer (accessed April 01, 2025).
(75) Meier, T.; Zhao, Y.; Chernyak, V.; Mukamel, S. Polarons, localization, and excitonic coherence in superradiance of biological antenna complexes. *J. Chem. Phys.* **1997**, *107*, 3876−3893.
(76) Moix, J. M.; Zhao, Y.; Cao, J. Equilibrium-reduced density matrix formulation: Influence of noise, disorder, and temperature on localization in excitonic systems. *Phys. Rev. B: Condens. Matter Mater. Phys.* **2012**, *85*, 115412.
(77) Jiang, T.; Ren, J.; Shuai, Z. Unified Definition of Exciton Coherence Length for Exciton−Phonon Coupled Molecular Aggregates. *J. Phys. Chem. Lett.* **2023**, *14*, 4541−4547.
(78) Song, L.; Shi, Q. A new approach to calculate charge carrier transport mobility in organic molecular crystals from imaginary time path integral simulations. *J. Chem. Phys.* **2015**, *142*, 174103.
(79) Mondelo-Martell, M.; Brey, D.; Burghardt, I. Quantum dynamical study of inter-chain exciton transport in a regioregular P3HT model system at finite temperature: HJ vs H-aggregate models. *J. Chem. Phys.* **2022**, *157*, 094108.
(80) Giannini, S.; Blumberger, J. Charge transport in organic semiconductors: the perspective from nonadiabatic molecular dynamics. *Acc. Chem. Res.* **2022**, *55*, 819−830.
(81) Anderson, P. W. Absence of diffusion in certain random lattices. *Phys. Rev.* **1958**, *109*, 1492.




https://doi.org/10.1021/acs.jpcc.5c02232
J. Phys. Chem. C 2025, 129, 12520−12530